NORMALISATION OF CONTINUUM-REMOVED LUNAR SPECTRA. A. Grumpe[1], V. Zirin[1], F. Belkhir[1], C. Wöhler[1], [1]Image Analysis Group, TU Dortmund University, D–44227 Dortmund, Germany; {arne.grumpe | vladimir.zirin | fethi.belkhir | christian.woehler}@tu-dortmund.de

Introduction: A common technique of analysing lunar spectra is unmixing of the observed reflectance spectra into standard reflectance spectra of compositional endmembers [1]. Other approaches explicitly rely on the depths and/or positions of the minima of absorption troughs in order to identify specific minerals in the lunar soil (cf. e.g. [2, 3]).

Since the surface reflectance depends on the illumination and viewing geometry [4], which is in turn governed by the small-scale topography of the lunar surface, a normalisation of reflectance spectra to a reference illumination and viewing geometry (commonly: 30° incidence angle, 0° emission angle, 30° phase angle [5]) is necessary, requiring high-resolution topographic data. However, the lateral resolution of available lunar digital elevation models (DEMs) is lower than the lateral resolution of recent hyperspectral imagery, and they might not be pixel-synchronous with the hyperspectral images due to uncertain selenolocation [6].

In this study, we present a framework for the normalisation of continuum-removed M³ spectra with respect to illumination and viewing geometry. Especially, the phase angle dependence of the absorption wavelength and depth inferred from continuum-removed spectra is analysed.

Image registration and DEM construction: In order to improve the lateral resolution of existing DEMs, an extended photoclinometry and shape from shading algorithm is applied to the image data in combination with a DEM of lower lateral resolution (here: the GLD100 [7]) as proposed in [8]. Optionally, the lateral resolution may be further increased by applying the algorithm presented in [9] to the resulting DEM.

The construction of DEMs from multiple radiance images highly depends on the pixel synchronity of the images, while image sets with strongly varying illumination conditions are favourable for DEM construction [8]. We found that M^3 images acquired during different orbits show misregistrations of up to several kilometers. Therefore, an illumination-independent image registration method is required, where a complex transformation model has to be applied since translations, rotations, and perspective distortions are apparent.

Illumination independence is achieved by 3D reconstructions based on single images, which transform the radiance images into DEMs as proposed in [8]. In order to cope with the perspective distortions, images of features obtained from the constructed single-image DEMs, e.g. surface inclination angles or directional surface gradients, are derived and overlaid on the GLD100. The resulting 3D object is projected into the camera on the spacecraft, where the corresponding transformation is given by the camera position and orientation. These parameters are determined by minimising the Euclidean distances between corresponding control points in the images or by maximising the mutual information between the features across the images (cf. Fig. 1). Due to inaccuracies in the DEM and possibly non-constant spacecraft motion behaviour during image acquisition, the image registration can be refined by additionally applying a second-order polynomial transformation to the output of the 3D approach.

Normalisation of Spectral Data: After removal of the thermal emission component (cf. [10] or [11]), the observed reflectances are normalised to reference geometry based on the Hapke AMSA model [4] using the lunar parameters determined in [12] and the single-scattering albedo estimated pixel-wise using the DEM, and based on the empirical photometric function proposed by Hicks et al. [13]. Optionally, the distortion of the spectra due to small-scale topography can be compensated using the empirical method proposed in [11, 14]. This correction cannot be achieved with the phase angle dependent approach in

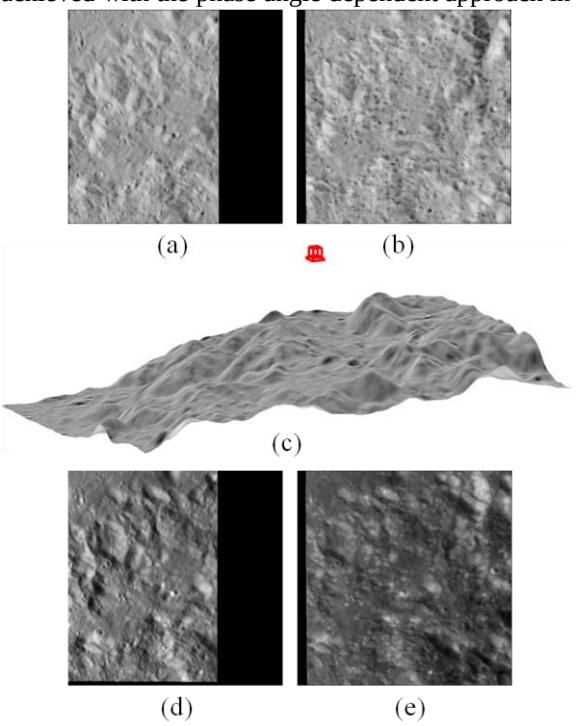

Fig. 1: Image Registration. Surface feature images (a) and (b) are extracted from single M³ radiance images. (c) The feature image is overlaid on the DEM and projected into the camera. The extrinsic camera parameters are determined and used to register the reflectance images (d) and (e) inferred from the M³ radiance images.

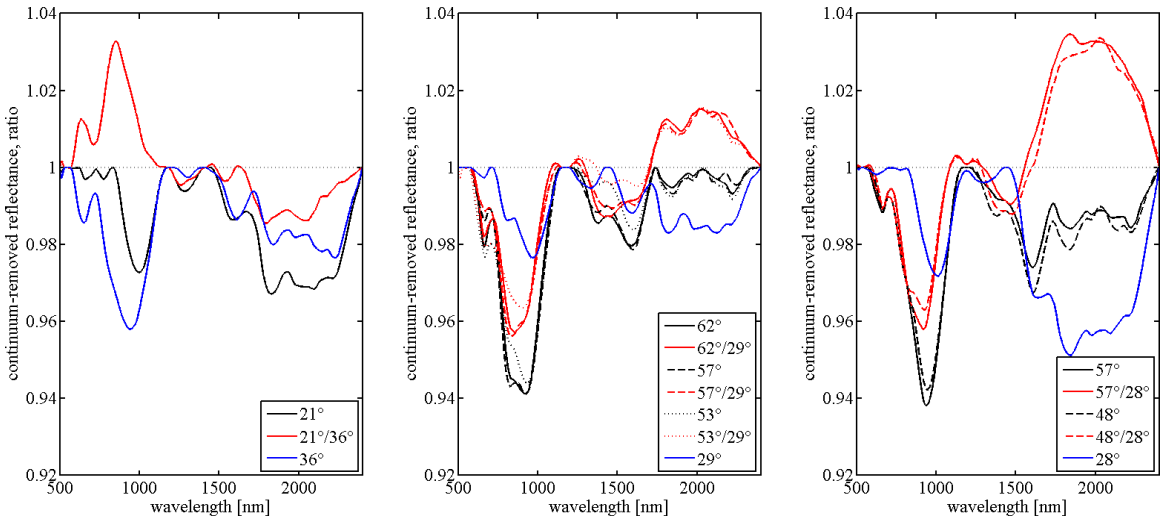

Fig. 2: Continuum-removed reflectance spectra and ratio spectra for the three test regions (left: 26–28°S, 116–118°E; centre: 17–19°S, 253–255°E; right: 15.6–17°N, 15–16.6°E). The numbers indicate phase angle values.

[13] as the phase angle is almost constant in the regarded images. The continuum of the spectrum is removed based on the convex hull approach [15]. For each of the three regarded test regions, four even (surface slope < 2°) subregions of 300 x 300 m^2 size were selected based on the constructed DEM.

For each test region, Fig. 2 shows the continuum-removed smoothed reflectance spectrum of one subregion and its ratio with respect to the spectrum acquired at the phase angle α_0 closest to 30°, for normalisation with the Hapke AMSA model [4].

Fig. 3 shows the shift $\Delta\lambda_{abs}$ of the absorption wavelength λ_{abs} of the absorption trough around 1000 nm and the relative variation δ/δ_0 of the band depth δ with changing phase angle α for the troughs around 1000 nm and 2000 nm. The relative band depth variations are computed as the ratios between the values of δ for the given phase angle α and for the phase angle α_0, respectively, where $\Delta\alpha = \alpha - \alpha_0$. The error bars denote the standard deviations over the subregions. The fitted curves are bias-free polynomials of 2nd order for $\Delta\lambda_{abs}$ and of 1st and 2nd order in the logarithmic scale for the depths of the absorption troughs at 1000 nm and 2000 nm, fitted to the averages over the subregions. For normalisation based on the Hapke AMSA model [4] with wavelength-independent (except for the single-scattering albedo) parameters, with increasing phase angle α the value of λ_{abs} becomes smaller, the depth of the 1000 nm trough increases, and the depth of the 2000 nm trough decreases. In contrast, the normalisation by Hicks et al. [13] based on wavelength-dependent parameters leads to a bimodal distribution of $\Delta\lambda_{abs}$ for $\Delta\alpha > 20°$, resulting in high fluctuations across the subregions, while both absorption depths decrease with increasing phase angle.

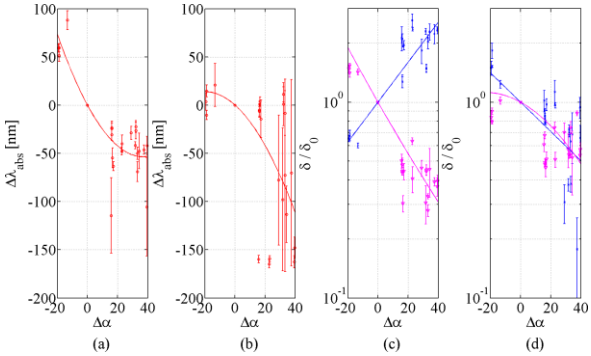

Fig. 3: Phase angle dependence of the variation $\Delta\lambda_{abs}$ of the absorption wavelength of the trough around 1000 nm (red) and the band depth ratio δ/δ_0 (blue: 1000 nm, magenta: 2000 nm trough) after normalisation using the Hapke AMSA model [4] ((a) and (c)) and the model by Hicks et al. [13] ((b) and (d)).

Conclusion: The observed absorption wavelength and band depth variations have been found to be phase angle dependent. Therefore, the normalisation of continuum-removed spectra can be refined either by applying an empirical correction to the extracted spectral features (cf. Fig. 3) or by performing a normalisation based on the Hapke AMSA model with appropriate wavelength dependent parameters.

References: [1] Mustard, J. F. and Pieters, C. M. (1988). *J. Geophys. Res. 94*, 13619-13634. [2] Matsunaga, T., et al. (2008) *Geophs. Res. Lett. 35*, L23201; [3] Bhatt, M., et al. (2011) *EPSC-DPS2011*, abstract #441; [4] Hapke, B. W. (2002) *Icarus 157*, 523–534. [5] Pieters, C. M. (1999) *Workshop New Views of the Moon 2*, 47. [6] Boardman, J. W., et al. (2011) *J. Geophys. Res. 116*, E00G14. [7] Scholten, F., et al. (2011) *LPSC XXXXII*, abstract #2046. [8] Grumpe, A. and Wöhler, C. (2011) *Proc. 7th IEEE Int. Symp. Image and Signal Processing and Analysis*, 609–614. [9] Grumpe, A. and Wöhler, C. (2012) *LPSC XXXXIII*, abstract #2597. [10] Clark, R. N., et al. (2011) *J. Geophys. Res. 116*, E00G16. [11] Wöhler, C. and Grumpe, A. (2012) *In: Innovations for Shape Analysis: Models and Algorithms. Rev. contrib. to Dagstuhl Seminar*, to appear. [12] Warell, J. (2004) *Icarus 167*, 271–286. [13] Hicks, M. D., et al. (2011) *J. Geophys. Res. 116*, E00G15. [14] Wöhler, C. and Grumpe, A. (2012) *LPSC XXXXIII*, abstract #1906. [15] Fu, Z., et al. (2007) *IEEE Trans. Geoscience and Remote Sensing 45(11)*, 3827–3844.